EUROPEAN COMMISSION

Community Research

Contract no.: 248231

MOSARIM

D2.4 - SIMULATION SETUP ASSESSMENT: INTERFERER – FREE SPACE PROPAGATION – VICTIM RADAR

Report type	Deliverable
Work Group	WP2
Dissemination level	Public
Version number	Version 1.0
Date	2011-12-22
Lead Partner	Karlsruhe Institute of Technology

Project Coordinator

Dr. Martin Kunert
Robert Bosch GmbH
Daimlerstrasse 6
71229 Leonberg
Phone +49 (0)711 811 37468
martin.kunert2@de.bosch.com

copyright 2011

the MOSARIM Consortium

Authors

Name	Company
Tom Schipper	Karlsruhe Institute of Technology

Revision chart and history log

Version	Date	Reason
0.3	2011-12-01	Initial version
0.4	2011-12-06	Additional text and simulations
0.9	2011-12-12	Enhancements based on input from project partners
0.95	2011-12-20	Peer review version
0.99	2011-12-21	Change with respect to results of peer review
1.0	2011-12-22	Final version for submission

Table of contents

1. Introduction

In MOSARIM milestone MS1 [MOSARIM1] information about which radars could interfere with each other was collected. In Deliverable D2.2 [MOSARIM2] the general simulation approach was described in more detail and susceptibility models were introduced. In Task 2.3 a collection of typical, ideal street scenarios was created which serves as a pool for feeding more realistic simulations containing a lot more boundary conditions than only the surface of a street.

In this Deliverable D2.4, before the interference situation on the streets is systematically investigated by more expensive simulations, the existing simulation approach has to be checked on its validness and ability to model interference effects. This check is done by comparing measurement results of a FMCW radar prototype that is interfered by a CW source in an anechoic chamber with simulation based on tools established and improved during the course of the MOSARIM project.

This document is structured in:

Chapter 1 - Introduction

Chapter 2 - Hardware setup for measurements

Chapter 3 - Simulation Overview
This chapter provides an overview of the structure which enables the simulation of multiple-interfering scenarios, followed by a short description of the “analog” signal processing in the used FMCW receiver used to get the simulation results.

Chapter 4 - Comparison: Measurement and Simulation
The comparison is conducted for:

- a setup with a single corner reflector as target
- a setup with absorbers in front of the victim radar, emitting a CW signal to observe the noise floor
- a setup with a single CW interferer

The document is completed by Conclusions and an Outlook on next steps.

2. Hardware Setup used for measurements

The radar used for measurements is a 8x8 digital beam-forming FMCW radar (*Fig. 1*) [HARTER1] with identical hardware components for all of the 8 receivers. This radar was used because it was developed by a member of the KIT RF institute and all details from signal generation to hardware are therefore well known. *Table 1* lists details about the system settings used for the measurements. *Table 2* shows hardware details of the receiver.

Fig. 1: 8x8 Digital Beamforming Radar

Description	**Value**
Transmit Power (EIRP)	20 dBm
Carrier Frequency	24,125 GHz
Sweep Bandwidth (BW)	250 MHz
Number of Rx channels	8
Switched Tx channels	8
Sweep time (t_{block})	2.5 ms for each ramp
Ramp type	Up-ramp
ADC sampling frequency	240 kHz
ADC resolution	14 bit

Table 1: System settings

Component	**Gain/Loss**	**Noise**
G_{TX}, G_{RX}	10 dB, loss of hard-wired cables included	-
LNA	G_{LNA} = 13 dB	NF_{LNA} = 3,5 dB
Mixer	L_{MIX} = 8 dB	NF_{MIX} = 8 dB
Active Bandpass Filter	A_{AAF} (passband):2430 V/V, f_{3dB} ~ 33 kHz	passband: 2.386 nV/(Hz$^{1/2}$)

Table 2: Hardware details

Based on the data listed in tables 1 and 2, the radar can achieve a range resolution of

$$\Delta R = \frac{c_0}{2 \cdot BW} = \frac{3 \cdot 10^8 m/s}{2 \cdot 250 MHz} = 0.6 m$$

and a Doppler resolution of

$$Df_d = \frac{1}{t_{block}} = \frac{1}{2.5 ms} = 400 Hz$$

In the tests performed no moving target exists, so the radar measures objects in distances up to

$$s_{\max} = \frac{f_{beat} \cdot c_0 \cdot t_{block}}{2 \cdot BW} = 82{,}5 m$$

where the maximum beat-frequency f_{beat} is assumed to be f_{3dB} = 33 kHz.

3. Simulation Overview

3.1. Mapping of scenario information

Because the simulation should support any numbers of radars, care was taken to ensure reliable storage of scenario information. *Fig. 2* illustrates this mapping procedure.

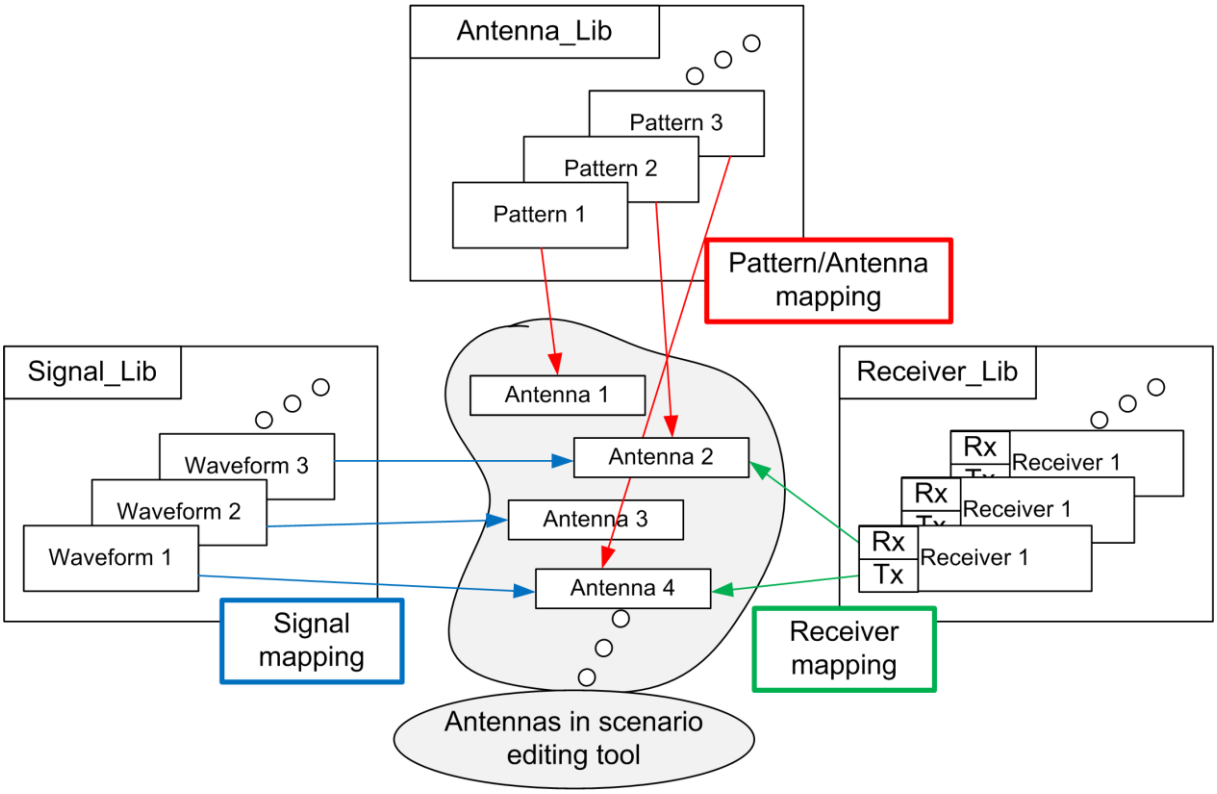

Fig 2: Basic scenario information mapping

Based on the information collected during the mapping procedure the following operations can be performed:

- Raytracing can be performed for all R_x – T_x combinations, or for any subset. This is started from Matlab™, where the workload is automatically distributed to the amount of CPU-cores as desired.
- Antennas are post-processed based on the data stored in the antenna-map
- Antennas are connected with waveform-objects, which contain information about the signal to be generated
- A channel object can be created, which always holds the information of one certain R_x antenna, and an arbitrary list of T_x antennas.

```
Channel(    ImpulseResponseResultFolder,... % storage of raytracing-results, choose with or without applied antennas
            rxAntennaList(1), ...           % take first Rx Antenna in list (antenna path from mapeditor = all antennas unique)
            txAntennaList(:), ...           % consider all Tx Antennas in the whole scenario (all potential interferers)
            SignalLookUpTable,...           % signal lookup-table
            ReceiverLookUpTable...          % receiver lookup-table
                        )
```

Alternatively the third argument can be called with *txAntennaList(4:10)*. This would lead to a channel where only T_x antennas with number 4 to 10 out of *txAntennaList* are considered.
If a channel-object recognizes that its R_x antenna and a T_x antenna are stored in a receiver-map, this antenna pair is handled as a radar (this is an absolutely universal approach).

The channel objects offer all important mechanisms for signal processing up to the ADC output (if detailed time domain simulation is done) or only up to the antenna port of the receiver with path loss only. Also a worst case interference level can be calculated. The signal processing is done for every snapshot with a separate call of the channel-object functions, so it can benefit from parallel processing.

3.2. Realisation of a simple FMCW receiver

The incoming signals are generated as complex signals in baseband in the following way (example for FMCW signal):

$$signal = ComplexChirp(...) \cdot \sqrt{2 \cdot R \cdot P_{\mathrm{Receive}}}$$

where R is 50 Ω and P_{Receive} is the receive Power at receive-antenna port where antennas are already considered. Used receive signals are delayed by adding zeros in front of the vectors according to the signal travelling time

signal = [zeros(1,ceil(timeDelay/samplingtime)) signal]

while at the beginning of channel generation a common sampling time is determined.
If signals are classified as interfering signals, these signals are periodically repeated, where a pause between the interfering ramps can be considered. (The initial ramp position can be random or is fixed)

Then all signals are scaled according to their channel impulse responses

$$signal = signal \cdot amplitude_{Pol} \cdot \exp\left(j \cdot phase_{Pol}\right)$$

where “Pol” is an index to pick the desired polarization. The signals are then shifted in frequency, dependent on their Doppler shift

$$signal = signal \cdot \exp\left(-j \cdot 2\pi \cdot f_{Doppler} \cdot t\right)$$

Now all signals are added up at the receiver

$$sumSignal = \sum_i signal_i$$

and are first amplified (simple multiplication, maybe also with saturation effect), mixed (signal .*conj(loSignal).*(loss,$gain_{V/V}$)) and filtered (filter is here implemented on basis of a netlist). After the filtering process a downsampling occurs that is followed by quantization to introduce some quantization noise.

4. Comparison: Measurement and Simulation

The prototype radar measurements are performed in an anechoic chamber at KIT (*Fig.3*) premises in Karlsruhe with suitable absorbers in place.

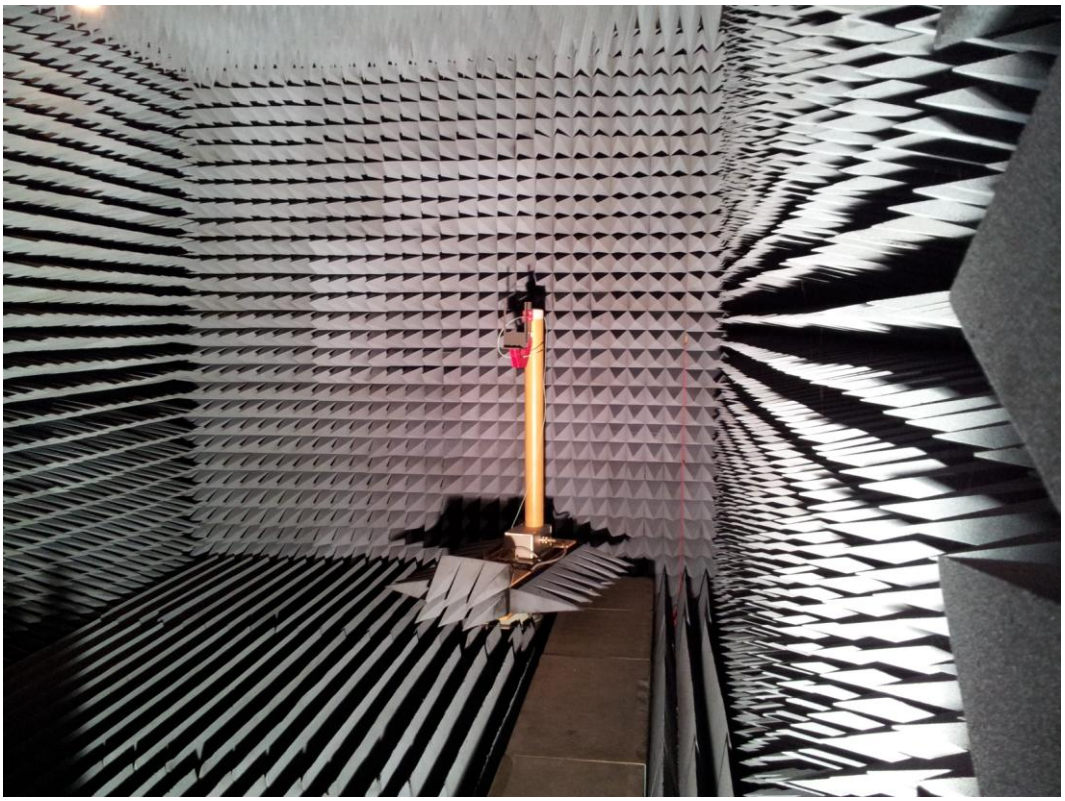

Fig. 3a: Anechoic chamber used for measurements

The platform with the tower holding the antenna in *Fig.3a* is equipped with removable absorbers. For the measurements, additional absorbers were used to cover the remaining metal of the platform. To further reduce clutter, an absorber was placed directly behind the mechanic, which holds the corner reflector or interfering antenna. The distance from the victim antennas to the corner reflector / interfering antenna was measured based on a commercial laser distance measurement tool.

4.1. Verification of use-signal power level

Fig.4 illustrates the measurement setup for a monostatic radar scenario with a single target (synthetic corner reflector with 2,885 dBsm). With respect to the system settings given in Table 1 and 2 the received power level at the receive-antenna port can be expressed to:

$$P_{RX} = P_{TX} + G_{RX} + 20\log_{10}\left[\frac{c_0}{f_c}\right] + s_{dBsm} - 10\log_{10}\left[(4p)^3 r^4\right] = -69\,dBm$$

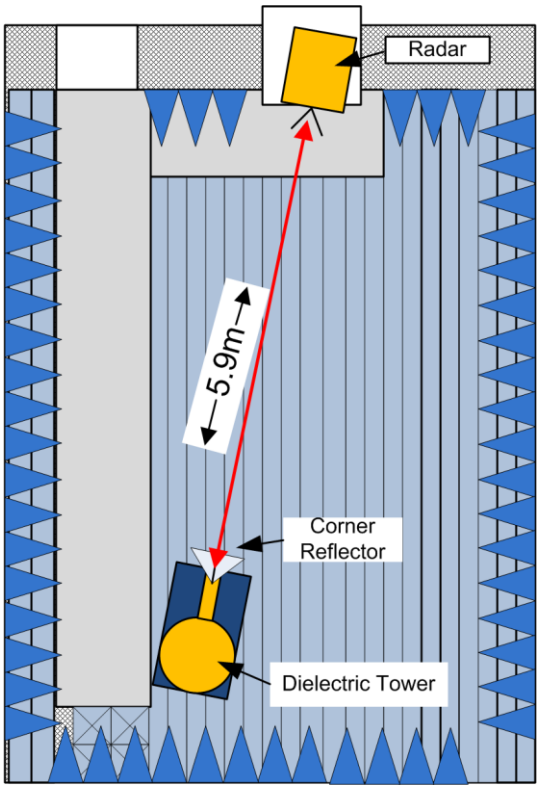

Fig. 4: Setup with corner reflector

Now applying LNA and Mixer Gains to get the input power of the AA-bandpass filter

$$P_{InAAF} = P_{RX} + G_{LNA} + L_{MIX} = -64dBm$$

Now the AA-filter amplification factor corresponding to the targets' beat frequency must be found. The effective beat frequency results from the signal runtime in freespace and from the cables to and from the antennas with an permittivity of ε_r=2

$$f_{beat} = \frac{2 \cdot s \cdot BW}{c_0 \cdot t_{block}} \Rightarrow \frac{2 \cdot 5.9\,m \cdot 250\,MHz}{c_0 \cdot 2{,}5\,ms} + \frac{0.7\,m \cdot 250\,MHz}{\frac{c_0}{\sqrt{2}} \cdot 2{,}5\,ms} = 3933{,}33\,Hz + 329{,}98\,Hz = 4263\,Hz$$

The corresponding gain of the bandpass filter at this frequency is 60,865 dB (=1104,7 V/V). With this information we can calculate the input voltage of the ADC

$$V_{ADC} = \sqrt{2 \cdot 50\Omega \cdot 10^{\frac{P_{InAAF}(dBW)}{10}}} \cdot 1104{,}7 = 0{,}22\ \text{V}$$ or -13,135 dBW (peak power at 1Ω)

Sampling is done with 240 kHz sampling rate, which leads to a signal vector with 601 points. *Fig.5* shows the measurement results (signal after ADC) in time domain and *Fig.6* the simulation results in frequency domain with an applied Hanning window.

Based on windowing and DFT, the displayed power level should be about -21,26 dB in frequency domain (what is currently not the case, although the signals amplitude in time domain are met quiet well).

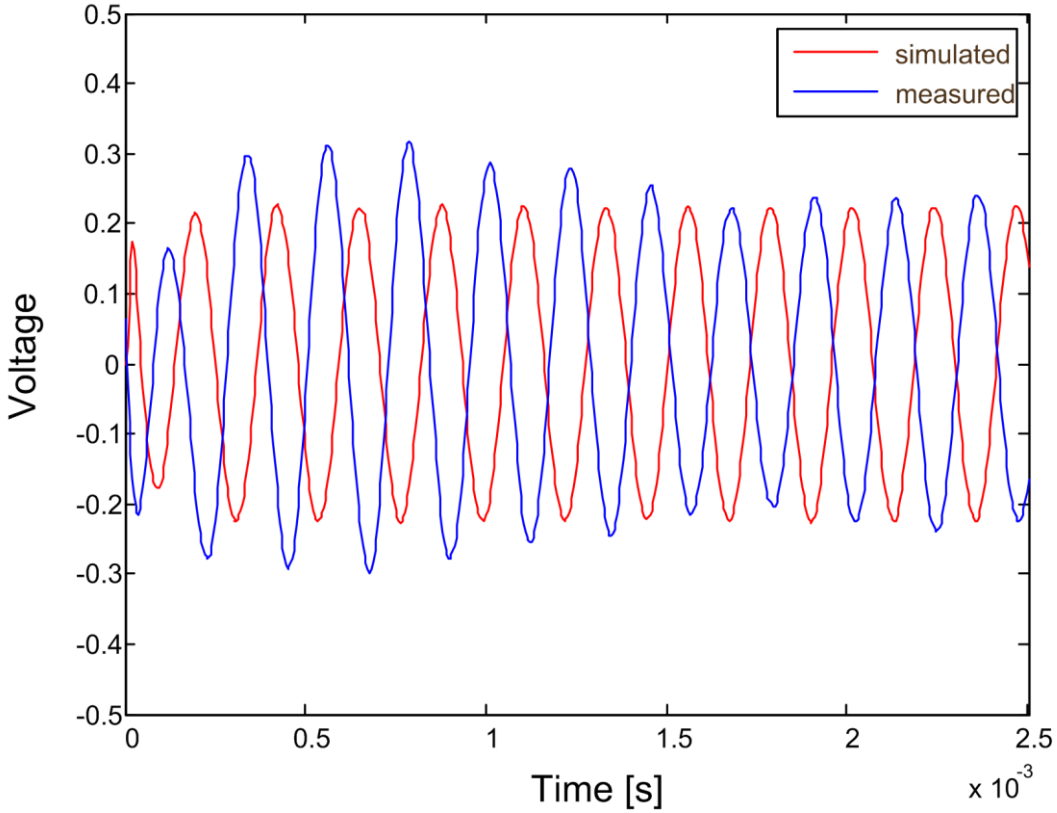

Fig 5: Comparison between measured and simulated signal in time domain

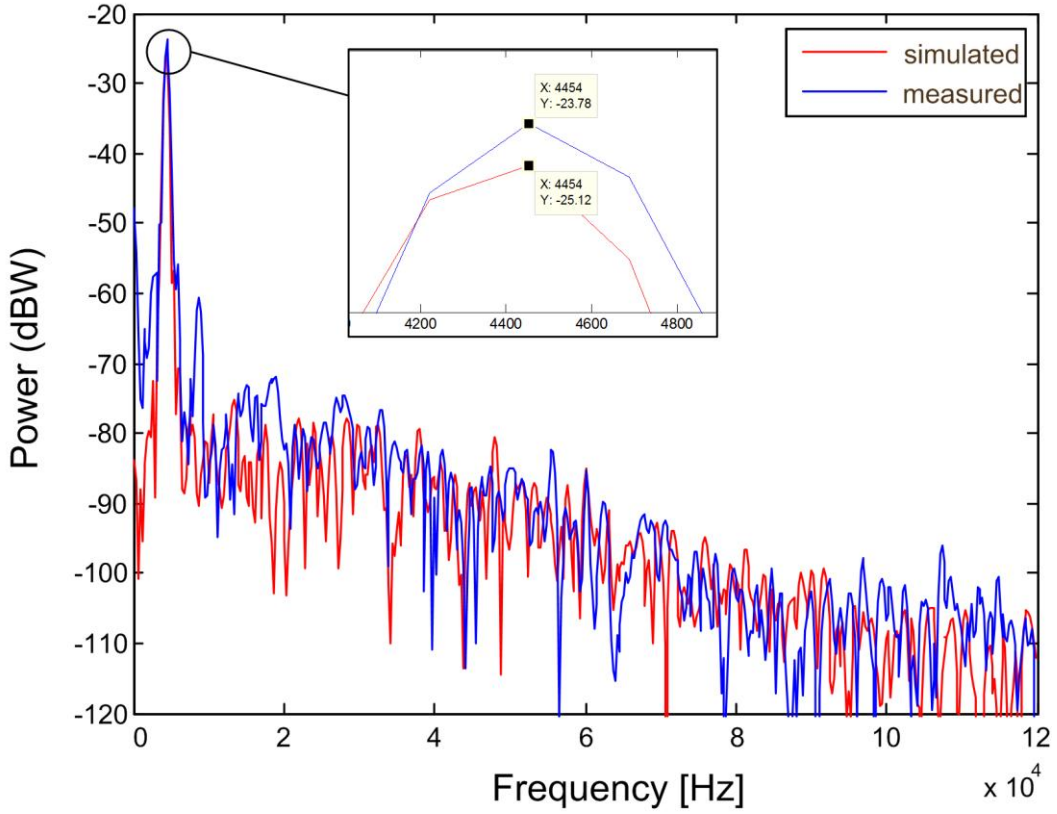

Fig 6: comparison between measured and simulated signal in frequency domain

4.2. Adding noise contribution

When feeding the simulation with basic receiver information such as bandwidth, temperature or noise figures of the single components, as well as with a more detailed, frequency dependent noise shape of the AA-filter an acceptable matching of the noise floor in the frequency domain (FFT) can be achieved for medium and higher frequencies. Low frequencies are more problematic due to finite isolations between signal lines and inside hardware components.

The initial noise contribution is inserted after the receive antenna as a voltage with $(KTBR)^{1/2}$, assuming perfect matching of antenna and LNA. All other components add their noise with respect to their bandwidth, their temperature and noise figure. The AA-bandpass filter, needed for avoiding aliasing and performing a compression of the dynamic for near distances, is modelled by taking its frequency dependent output noise voltage density, dividing this by the filters transfer function and add them directly on the filter-input signal so both signal and noise are filtered and amplified together. In this example the noise floor is adequate and results from contributions of the single hardware components, but even if there are more problems to match a noise floor of radars, frequency dependent noise can be directly added to generate a given S/N behaviour.

Fig.7 shows the results in time domain and *Fig.8* the results in frequency domain for the following setup:

- LO-Signal is configured as CW-Signal at 24.125 GHz
- A stationary absorber is placed directly in front of the T_x and R_x antennas

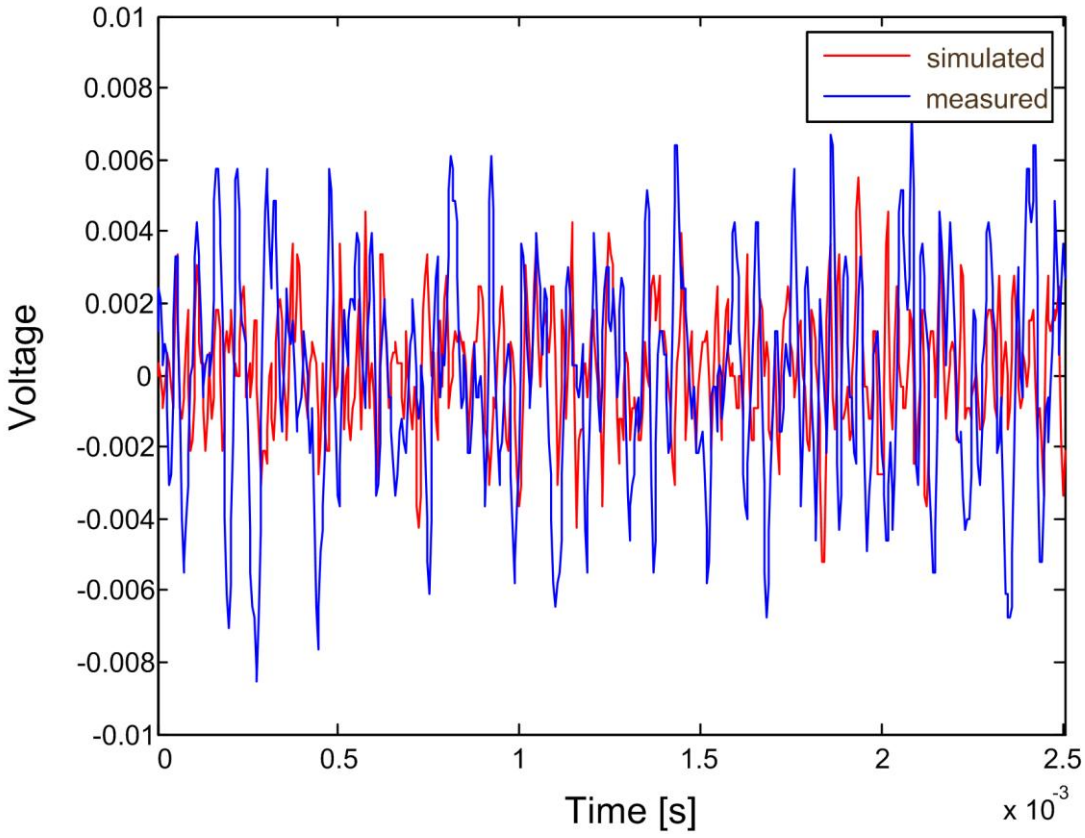

Fig 7: Generated noise in time domain after quantization

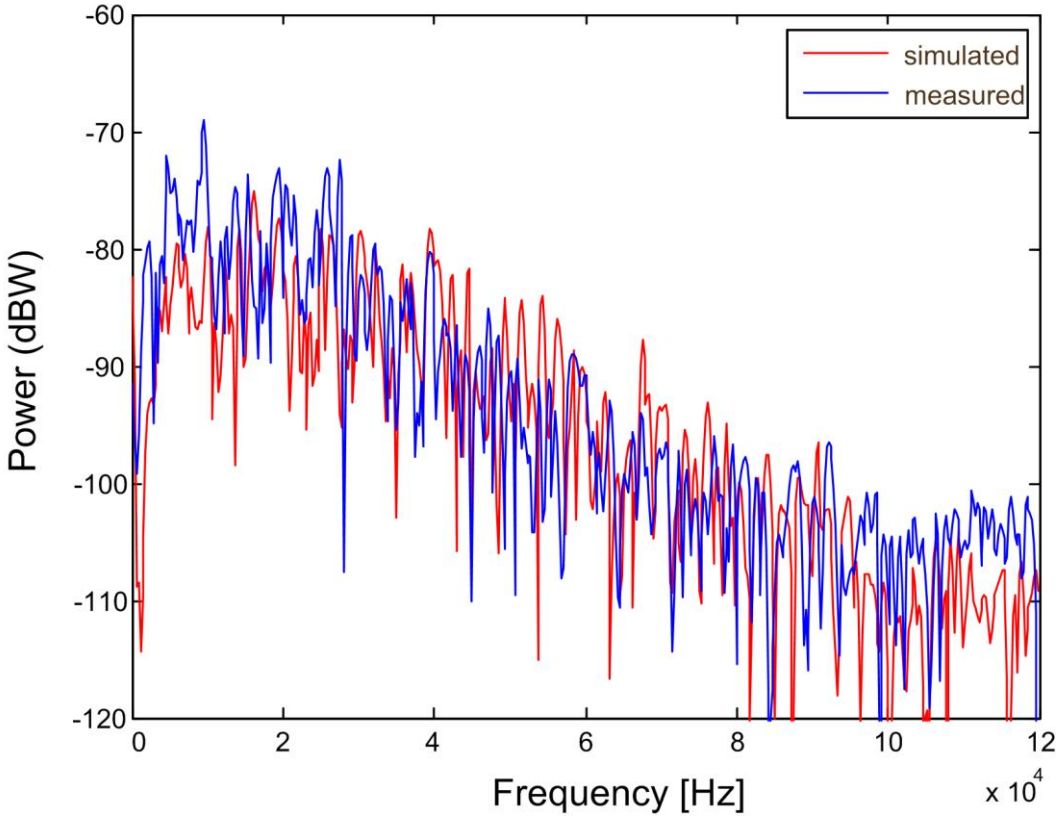

Fig 8: Frequency domain noise after quantization

4.3. Verification of interference power level

Fig.9 illustrates the measurement setup for an interfering scenario with a single interferer. The corner reflector from Fig.1 was physically removed and replaced by an interfering antenna. This interfering antenna is now directly illuminating the victim radar with 15 dBm EIRP at 24.125 GHz. The signal generator is hidden behind some additional absorber material.

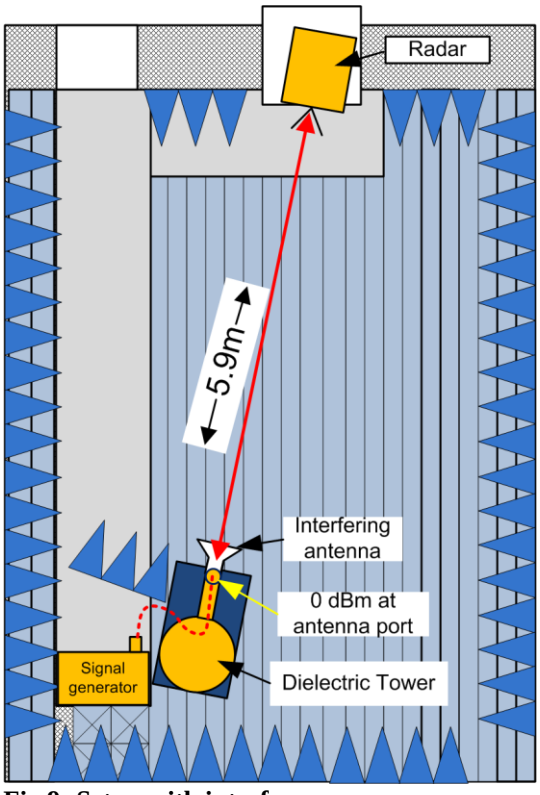

Fig.9: Setup with interferer

To mark the position of the interferer in simulation, the interfering antenna will be represented by the synthetic corner reflector already used in subsection 3.1. Due to this the use signal power level will not match with the one created by the physically present interfering antenna. To apply interference mitigation techniques, it is useful to have some causal use signal power levels because one has to, for example, apply a “smooth” connection between the separated useful signal parts. But as it is later shown, the presence of a use signal is not a must have to visualize the interference effects.

Fig. 10 to12 show selected measurement and simulation results; “selected” because ramps were chosen out of the measurements, where the phase between victim LO and interfering radar are matching the simulations. This phase relation between victim LO and interfering signal determines if the corresponding interfering-peak is pointing upwards, downwards or is reduced in amplitude. The simulation results at this point are satisfying and enable the reproduction of the measurements. For lower frequencies the alignment of simulation and measurement gets worse, because of dynamic DC-offset effects.

In *Fig. 13* and *Fig. 14* it is demonstrated that the measurement results can be matched to simulation by a successive shift of the initial phase of the interfering signal.

Fig. 15 shows further measurement and simulation results, but with simulated victim transmitter switched off (no use signal is generated in simulation). This figure demonstrates that the interference effects can be investigated in general also without any presence of a use signal.

Viewing the interference floor in frequency domain for 8 victim ramps in a row with CW interference always activated, it is clearly visible that the occurring interference floor is fluctuating over a huge dynamic range. *Fig.16* shows the time domain results, *Fig.17* shows the results in frequency domain. This figure underlines the random behaviour of the noise floor as a function of the phase relation between LO and interfering signal.

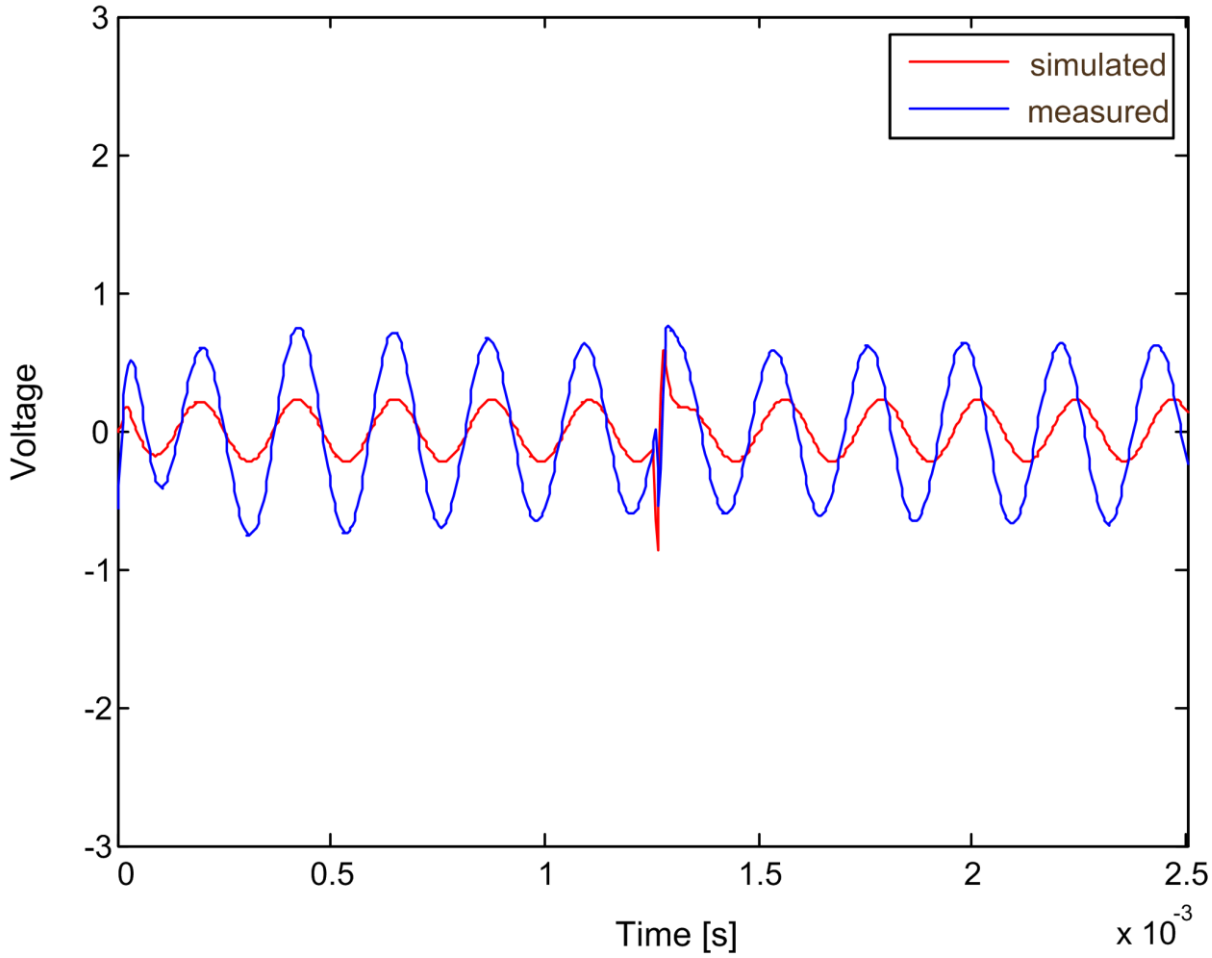

Fig. 10: Complete time domain signal, measured and simulated

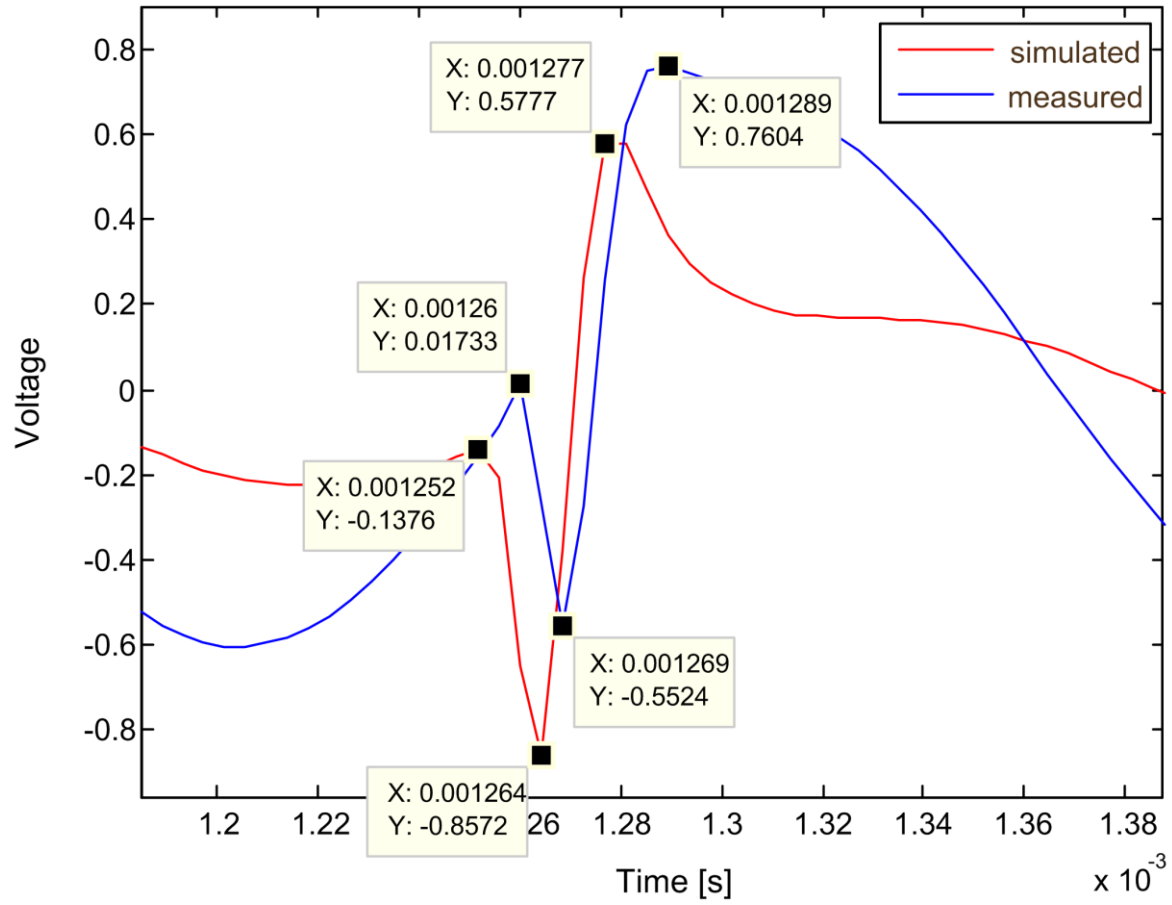

Fig. 11: Zoom into time domain interference effect from Fig. 8

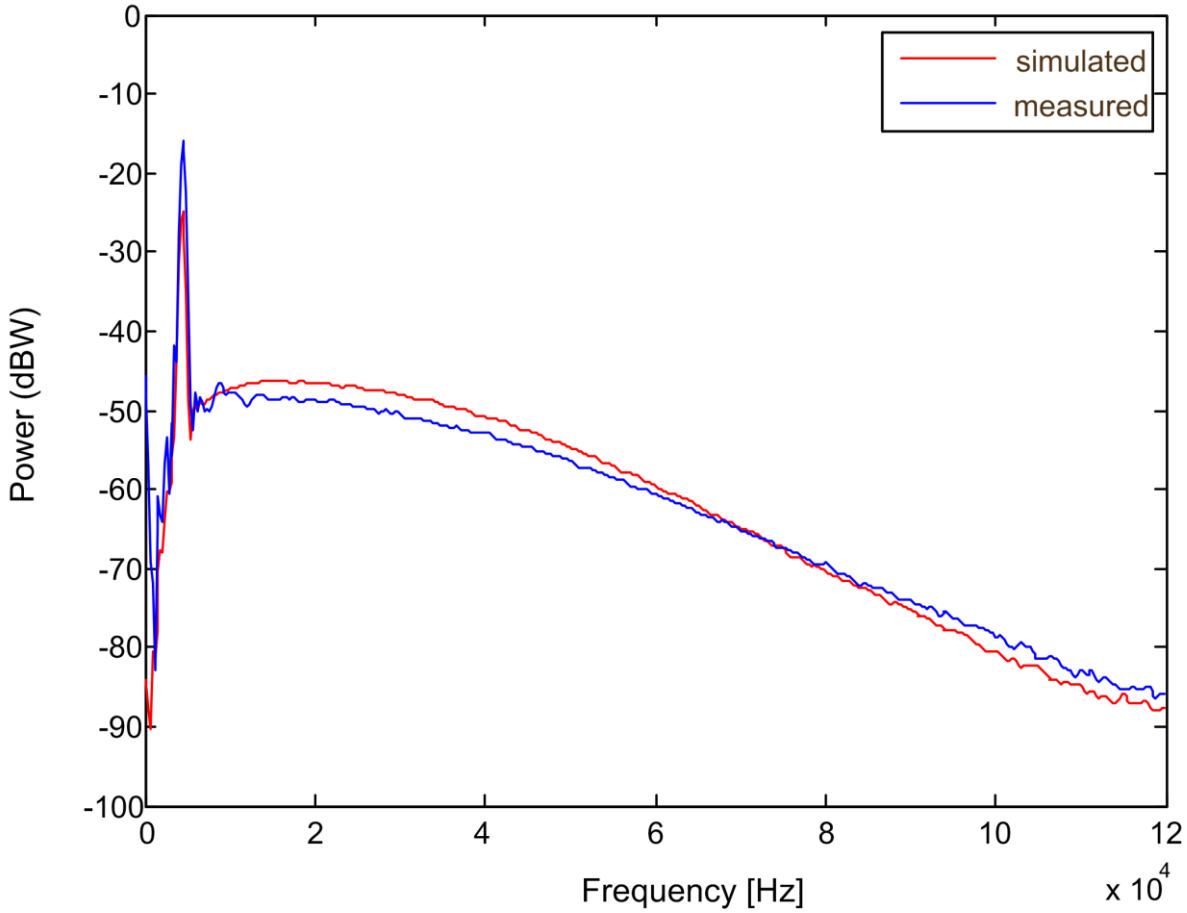

Fig. 12: Interference effect in frequency domain

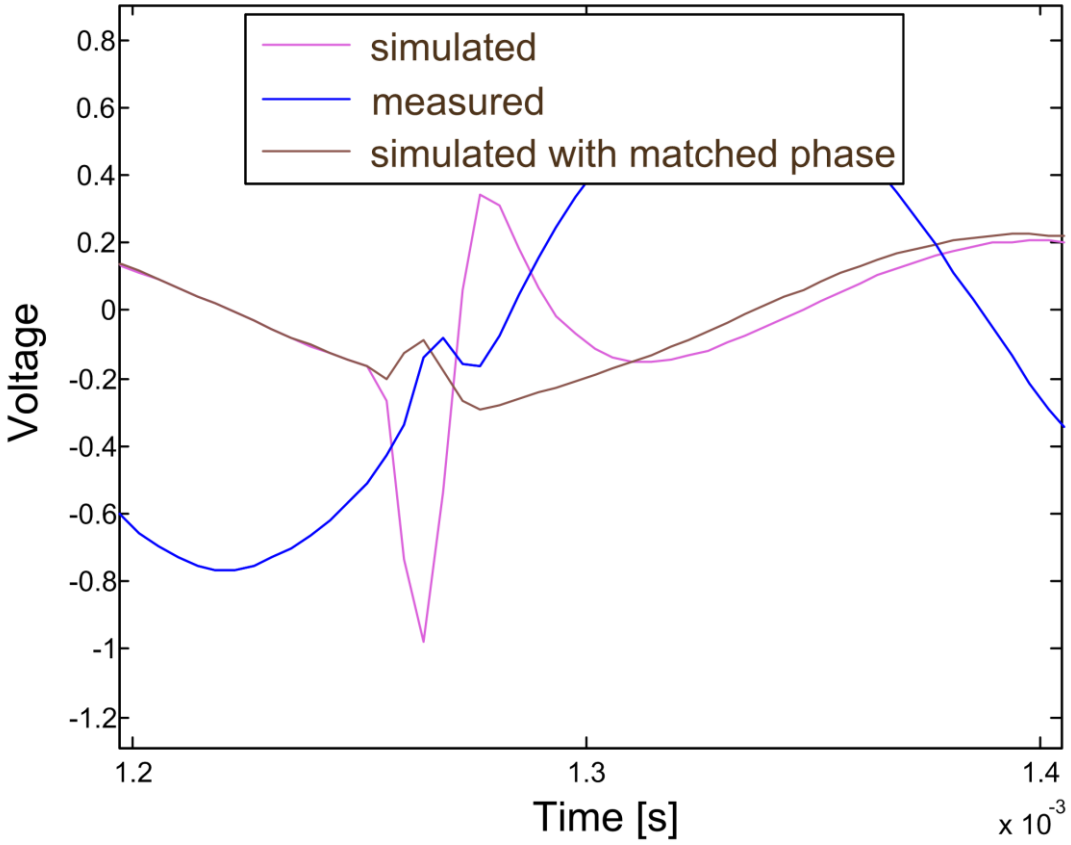

Fig 13: The measured time domain result can be reached by shifting the phase of the interfering signal

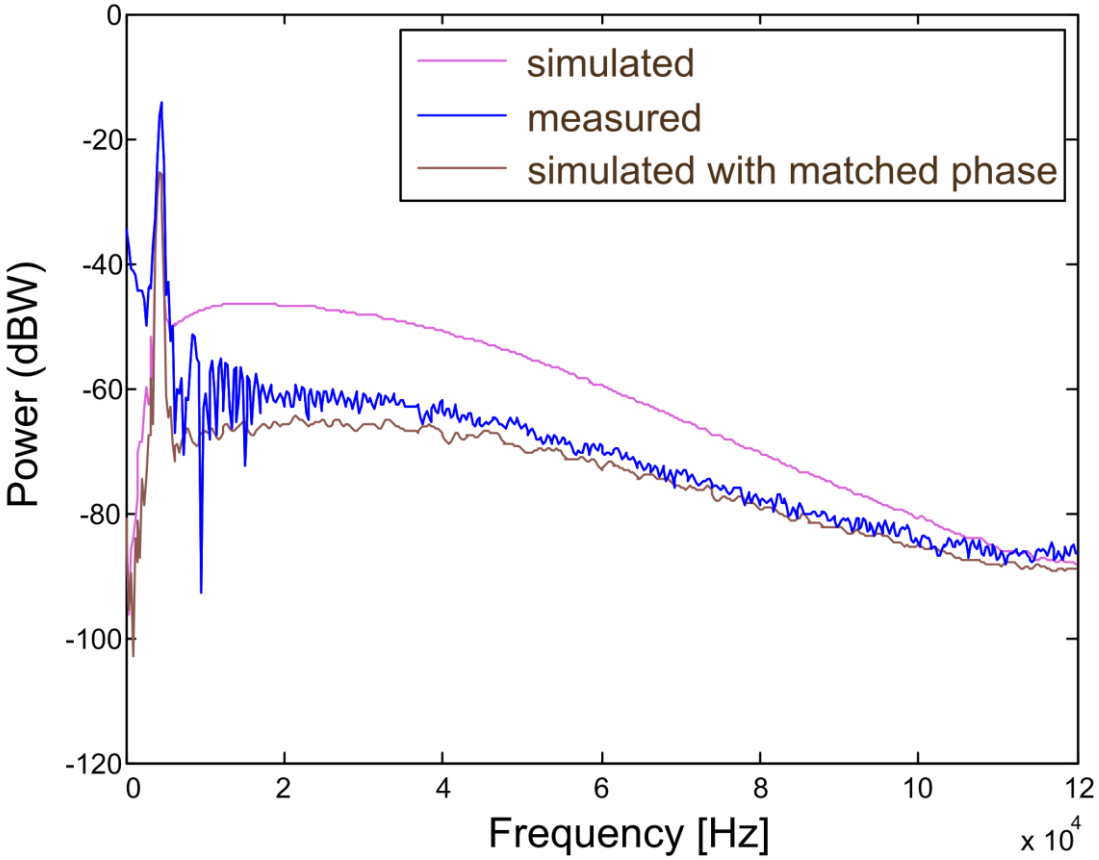

Fig 14: The measured frequency domain result can be reached by shifting the phase of the interfering signal

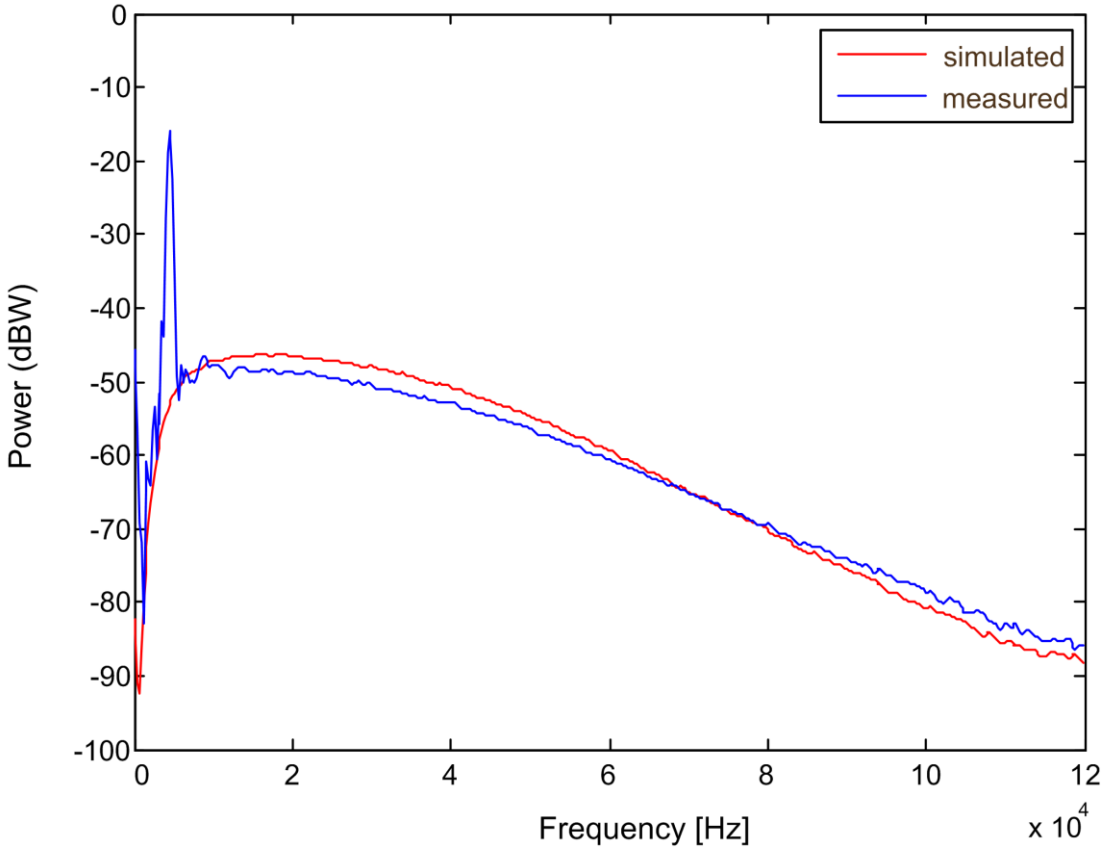

Fig 15: The interference effect can also be demonstrated without the presence of a use signal

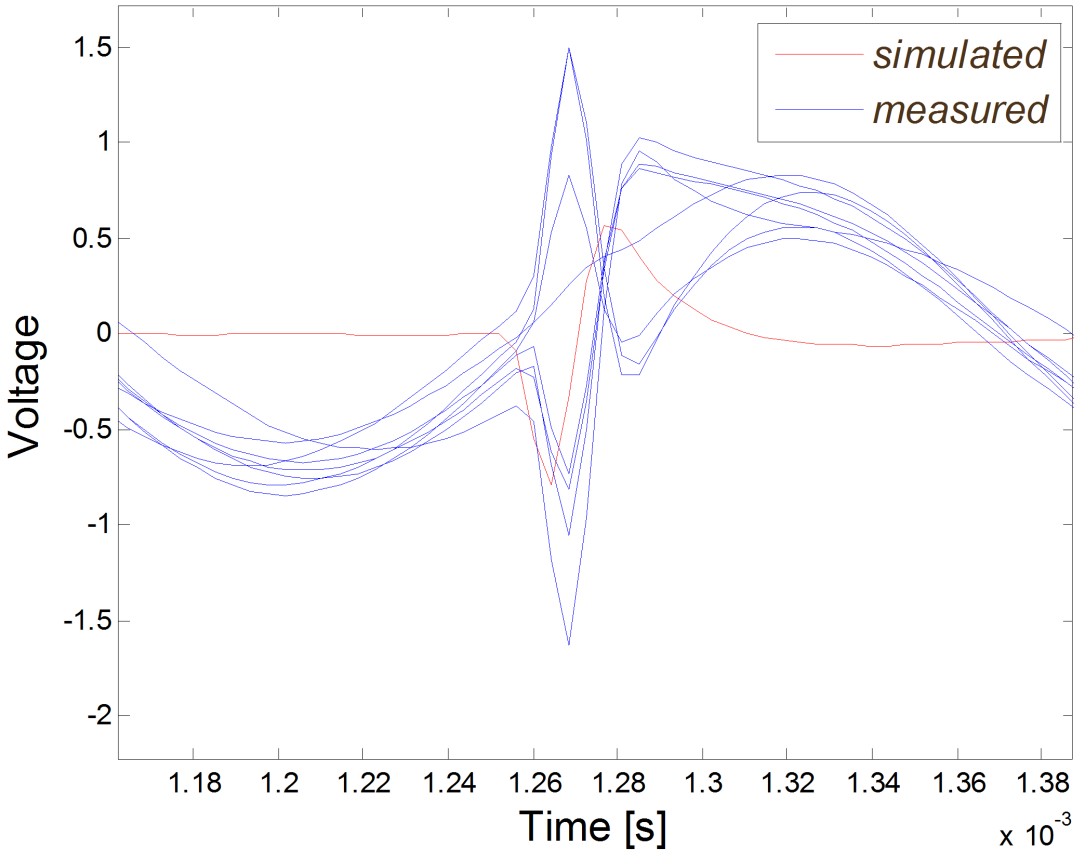

Fig 16: Array of curves for 8 stored victim radar ramps in a row. The changing phase of the interfering signal leads to different appearances of the resulting peak.

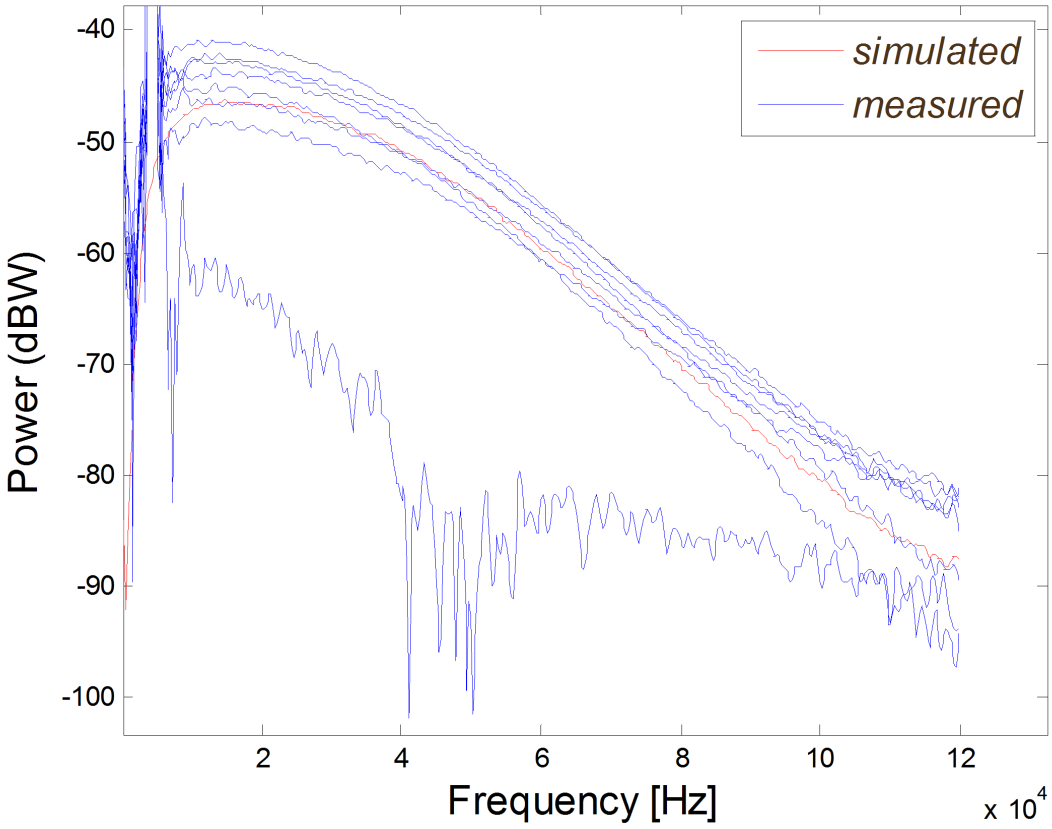

Fig 17: Array of curves for 8 stored victim ramps in a row.

5. Conclusions

In this deliverable a simple free-space model setup is used to show that the current version of the simulation system can be reliably used to reproduce interference effects. In general it can be concluded that interference effects can be reproduced by simulation, and even if they are not absolutely in alignment with measurements because of the many varying system parameters, the relative comparison within the simulator is possible in any case. Because of the fluctuating of the interference dependent on different phases, worst case interference estimations will play also an important role as well as the estimation of common interference levels (including probability aspect).

However, this first validation performed and described in this report is just a snapshot. Further validation tests must be and are done in parallel while continuing software-development.

Furthermore, the simulation environment has reached a level of confidence that makes it possible to do useful interference simulations with an arbitrary number of radars. There is still the potential to increasing the level of detail regarding hardware modelling in the respective simulation tools.

6. References

[HARTER1] M. Harter, A. Ziroff, T. Zwick, "Three-Dimensional Radar Imaging by Digital Beamforming", in European Radar Conference (EuRAD), Manchester, UK, Oct. 2011.

[MOSARIM1] Milestone Document 2.1, “Establishing of a common interference interaction matrix and evaluation factors”, EU project MOSARIM, Contract no.: 248231

[MOSARIM2] Deliverable 2.2, “Generation of an interference susceptibility model for the different radar principles“, EU project MOSARIM, Contract no.: 248231

7. Abbreviations

AAF	Anti Aliasing Filter
ADC	Analog to Digital Converter
BW	Bandwidth
CPU	Central Processing Unit
CW	Continuous Wave
DC	Direct Current
EIRP	Equivalent Isotropic Radiated Power
FMCW	Frequency Modulated Continuous Wave
G	Gain
L	Loss
LO	Local Oscillator
LNA	Low Noise Amplifier
RX	Receiver
TX	Transmitter